Large area photonic crystal cavities: a local density approach

M. C. F. Dobbelaar,[1,2] **S. Greveling,**[1,2] **and D. van Oosten**[1,2,*]

[1]*Debye Institute for Nanomaterials Science & Center for Extreme Matter and Emergent Phenomena, Utrecht University, Princetonplein 5, 3584 CC Utrecht, The Netherlands*

[2]*These authors contributed equally to this work*

[*]*D.vanOosten@uu.nl*

Abstract: Large area photonic crystal cavities are devices of interest for photovoltaics, optoelectronics, and solid-state lighting. However, depending on their dimensions they pose a large computational challenge. Here, we use a local density approach to avoid direct simulation of the device. We capture the effect of both ideal and distorted photonic crystals in an effective mass and an effective potential. We use these to map the problem of calculating the electromagnetic field modes to solving a simple time-independent Schrödinger equation. We show that, in the case that the hole radius varies quadratically as a function of position, the eigenmodes of the photonic crystals can be described by the corresponding eigenmodes of the quantum harmonic oscillator with typical agreements well above 90 %.

OCIS codes: (050.5298) Photonic crystals, (050.1590) Chirping.

References and links

1. J. D. Joannopoulos, S. G. Johnson, J. N. Winn, and R. D. Meade, *Photonic Crystals: Molding the Flow of Light* (Princeton University, 2008).
2. T. F. Krauss and R. M. D. L. Rue, "Photonic crystals in the optical regime past, present and future," Prog. Quantum Electron. **23**, 51 – 96 (1999).
3. J. R. Hook and H. E. Hall, *Solid State Physics* (John Wiley and Sons, 1991).
4. A. Bruyant, G. Lérondel, P. J. Reece, and M. Gal, "All-silicon omnidirectional mirrors based on one-dimensional photonic crystals," Appl. Phys. Lett. **82**, 3227 – 3229 (2003).
5. E. Istrate and E. H. Sargent, "Photonic crystal heterostructures and interfaces," Rev. Mod. Phys. **78**, 455 – 481 (2006).
6. T. Baba, "Slow light in photonic crystals," Nature Photon. **2**, 465 – 473 (2008).
7. A. A. Erchak, D. J. Ripin, S. Fan, P. Rakich, J. D. Joannopoulos, E. P. Ippen, G. S. Petrich, and L. A. Kolodziejski, "Enhanced coupling to vertical radiation using a two-dimensional photonic crystal in a semiconductor light-emitting diode," Appl. Phys. Lett. **78**, 563 – 565 (2001).
8. F. Pratesi, M. Burresi, F. Riboli, K. Vynck, and D. S. Wiersma, "Disordered photonic structures for light harvesting in solar cells," Opt. Express **21**, A460 – A468 (2013).
9. J. Skibina, R. Iliew, J. Bethge, M. Bock, D. Fischer, V. Beloglasov, R. Wedell, and G. Steinmeyer, "A chirped photonic-crystal fibre," Nature Photon. **2**, 679 – 683 (2008).
10. J. Knight, "Photonic crystal fibres," Nature **424**, 847 – 851 (2003).
11. R. Engelen, D. Mori, T. Baba, and L. Kuipers, "Two regimes of slow-light losses revealed by adiabatic reduction of group velocity," Phys. Rev. Lett. **101**, 103901 (2008).
12. D. Mori and T. Baba, "Wideband and low dispersion slow light by chirped photonic crystal coupled waveguide," Opt. Express **13**, 9398–9408 (2005).
13. M. Charbonneau-Lefort, E. Istrate, M. Allard, J. Poon, and E. Sargent, "Photonic crystal heterostructures: Waveguiding phenomena and methods of solution in an envelope function picture," Phys. Rev. B **65**, 125318 (2002).
14. J. Vigneron and V. Lousse, "Theory of chirped photonic crystals," Opt. Quantum Electron. **39**, 377 – 385 (2007).

#228367 - $15.00 USD Received 11 Dec 2014; revised 27 Jan 2015; accepted 9 Feb 2015; published 13 Mar 2015

15. B.-S. Song, S. Noda, T. Asano, and Y. Akahane, "Ultra-high-q photonic double-heterostructure nanocavity," Nature Mater. **4**, 207–210 (2005).
16. S. Mahmoodian, J. E. Sipe, C. G. Poulton, K. B. Dossou, L. C. Botten, R. C. McPhedran, and C. M. de Sterke, "Double-heterostructure cavities: From theory to design," Phys. Rev. A **86**, 043802 (2012).
17. C. Sauvan, G. Lecamp, P. Lalanne, and J. Hugonin, "Modal-reflectivity enhancement by geometry tuning in Photonic Crystal microcavities," Opt. Express **13**, 245 – 255 (2005).
18. S. Johnson and J. Joannopoulos, "Block-iterative frequency-domain methods for Maxwell's equations in a planewave basis," Opt. Express **8**, 173–190 (2001).
19. A. F. Oskooi, D. Roundy, M. Ibanescu, P. Bermel, J. D. Joannopoulos, and S. G. Johnson, "Meep: A flexible free-software package for electromagnetic simulations by the FDTD method," Comput. Phys. Commun. **181**, 687–702 (2010).
20. V. Mandelshtam and H. Taylor, "Harmonic inversion of time signals and its applications," J. Chem. Phys. **107**, 6756–6769 (1997).
21. D. J. Griffiths, *Introduction to Quantum Mechanics* (Pearson Education, Inc., 2005).
22. B. R. Johnson, "New numerical methods applied to solving the one-dimensional eigenvalue problem," J. Chem. Phys. **67**, 4086 – 4093 (1977).
23. E. Karimi, R. W. Boyd, P. de la Hoz, H. de Guise, J. Řeháček, Z. Hradil, A. Aiello, G. Leuchs, and L. L. Sánchez-Soto, "Radial quantum number of Laguerre-Gauss modes," Phys. Rev. A **89**, 063813 (2014).

1. Introduction

Photonic crystals are periodic dielectric structures which can exhibit a complete photonic band gap [1, 2]. This photonic band gap is analogous to the band gap observed in semiconductors [3]. The defining property of the photonic band gap is that it forbids propagation of light in a certain frequency range [1, 2]. This property enables full control and manipulation of light. This has led to many applications such as omni-directional mirrors [4], heterostructure cavities [5], slow light generation [6], photonic crystal LEDs [7], solar cells [8], (chirped [9]) photonic crystal fibers [10], and chirped photonic crystal coupled waveguides [11, 12].

For all these applications, the design of the photonic crystal device is crucial for the manipulation of light. However, designing and simulating large photonic crystals devices requires large computational power. Accurately capturing the effect of the periodicity requires a high resolution within the unit cell, which in a finite-difference time-domain (FDTD) calculation additionally leads to a very small time step. Furthermore, as one needs to simulate a large device, a large number of these unit cells have to be included in the simulation. This results in a very large memory usage and long simulation times which can span several days.

This problem can be overcome using slowly varying envelope approximations [13, 14], in which deviations from a perfectly periodic structure are treated perturbatively. We on the other hand obtain the envelope using a local density approximation. We summarize the effect of the band structure in terms of an effective mass and the energy of the bottom of the band of interest. We then use this energy as an effective potential for a massive particle and solve the wave equation for that particle. This amounts to solving the time-independent Schrödinger equation. In this way the microscopic problem is transformed into solving a macroscopic equation.

Here, we give a proof of principle of this method for one and two-dimensional photonic crystals of air holes, in the specific case that the hole radius varies quadratically as a function of position. For these systems we determine the overlap between the solutions of the time-independent Schrödinger equation and high resolution FDTD simulations. We show that our method can even take into account disorder due to fabrication imperfections which are always present in real photonic crystal devices. Our method offers more insight in the modes of large area photonic structures and greatly relaxes the computational effort in designing these structures. It therefore opens up new possibilities to design, develop and understand larger and more complex devices relevant to photovoltaics, optoelectronics, and solid-state lighting.

#228367 - $15.00 USD Received 11 Dec 2014; revised 27 Jan 2015; accepted 9 Feb 2015; published 13 Mar 2015

2. Theory

From Maxwell's equations for dielectric media with permittivity ε and permeability μ, the wave-equations for the electric and magnetic fields are given by [1]

$$\nabla \times \left(\frac{1}{\mu}\nabla \times \mathbf{E}\right) - \varepsilon k_0^2 \mathbf{E} = 0, \quad (1)$$

$$\nabla \times \left(\frac{1}{\varepsilon}\nabla \times \mathbf{H}\right) - \mu k_0^2 \mathbf{H} = 0, \quad (2)$$

where $k_0 = \sqrt{\varepsilon_0 \mu_0}\omega$ denotes the wavevector, ω the frequency, and ε_0 and μ_0 the vacuum permittivity and permeability, respectively.

In a medium where ε or μ vary periodically in space, *i.e.*

$$\varepsilon(\mathbf{x}+\mathbf{R}) = \varepsilon(\mathbf{x}) \text{ and } \mu(\mathbf{x}+\mathbf{R}) = \mu(\mathbf{x}),$$

where $\mathbf{R}$ is any lattice vector, it is well known that the eigenstates obey Bloch's theorem and thus take the form

$$\mathbf{E}_{m,\mathbf{k}}(\mathbf{x}) = \mathscr{E}_{m,\mathbf{k}}(\mathbf{x}) e^{i\mathbf{k}\cdot\mathbf{x}}, \quad (3)$$

$$\mathbf{H}_{m,\mathbf{k}}(\mathbf{x}) = \mathscr{H}_{m,\mathbf{k}}(\mathbf{x}) e^{i\mathbf{k}\cdot\mathbf{x}}, \quad (4)$$

with $\mathscr{E}_{m,\mathbf{k}}(\mathbf{x}+\mathbf{R}) = \mathscr{E}_{m,\mathbf{k}}(\mathbf{x})$ and $\mathscr{H}_{m,\mathbf{k}}(\mathbf{x}+\mathbf{R}) = \mathscr{H}_{m,\mathbf{k}}(\mathbf{x})$. Solving the wave equations using these functions as an ansatz, yields a set of eigenvalues k_0 for each $\mathbf{k}$ that correspond to the dispersion $\omega_{m,\mathbf{k}}/c$ of the Bloch bands.

The dispersion exhibits bands (labeled m) and band gaps. For our method we need an isolated band, the bottom of which does not overlap with other bands *i.e.* the first band above a band gap. In two dimensions the third TM band of a triangular lattice of air holes is a good example [1]. When one decreases the hole radius in a small region of the crystal the bands in this region shift down. This means that light can be trapped there. Famous practical examples of this mechanism are so-called double-heterostructure cavities [15, 16], and photonic crystal microcavities [17]. As these cavities are usually optimized to have a small mode volume they can be effectively simulated using FDTD methods. Large mode-area cavities on the other hand do not easily lend themselves to direct simulation.

However, when the mode-area is large, we can assume that the hole radius varies only slowly as a function of position and that the cavity mode thus samples only a small distribution of hole radii. In that case, we expect that we can to a good approximation find the eigenmodes of the cavity by simply multiplying the Bloch solutions by a scalar function $\Psi_n(\mathbf{x})$ that creates a slowly varying envelope for mode n. We thus write

$$\mathbf{E}_n(\mathbf{x}) = \Psi_n(\mathbf{x}) a^{3/2} \sum_{\{\mathbf{k}_{\min}\}} \mathscr{E}_{m_c,\mathbf{k}_{\min}}(\mathbf{x}) e^{i\mathbf{k}_{\min}\cdot\mathbf{x}}, \quad (5)$$

$$\mathbf{H}_n(\mathbf{x}) = \Psi_n(\mathbf{x}) a^{3/2} \sum_{\{\mathbf{k}_{\min}\}} \mathscr{H}_{m_c,\mathbf{k}_{\min}}(\mathbf{x}) e^{i\mathbf{k}_{\min}\cdot\mathbf{x}}, \quad (6)$$

where m_c denotes the number of the band used to create the cavity mode, and a the lattice constant. The summation is performed over all wavevectors $\mathbf{k}_{\min}$ in the first Brillouin zone that yield a minimum of the band.

The eigenmodes of the photonic crystal cavity can thus be described by the corresponding envelope $\Psi_n(\mathbf{x})$. To find this envelope without performing time consuming FDTD simulations, we use a local density approach. We first calculate the band structure for a photonic crystal

#228367 - $15.00 USD Received 11 Dec 2014; revised 27 Jan 2015; accepted 9 Feb 2015; published 13 Mar 2015

with a certain hole radius. From this band structure, we extract the bottom of the m_c-th band and the curvature at the bottom, which we express in terms of an effective mass. We repeat this calculation for a range of hole radii to obtain the frequency $\omega_0(\rho)$ at the bottom of the band and the effective mass $m^*(\rho)$ as a function of the hole radius ρ. As we will show, for a suitable choice of the system, the effective mass varies only weakly with hole radius. We therefore will assume that the effective mass is constant over the system. The bottom $\omega_0(\rho)$ on the other hand scales approximately linearly with the hole radius.

If we change the hole radius as a function of the position of the lattice vector $\mathbf{R}_i$, *i.e.* $\rho_i = \rho(\mathbf{R}_i)$, we can approximate the energy of light in the m_c-th band at that lattice vector as $E_i = \hbar\omega_0(\rho(\mathbf{R}_i))$, where $\hbar$ denotes the reduced Planck's constant. In the local density approximation, we now treat this position dependent energy as a potential energy

$$V(\mathbf{x}) = \hbar\omega_0(\rho(\mathbf{x})). \tag{7}$$

Note that in the above equation, we treat $\rho(\mathbf{x})$ as a continuous function, where before we only defined ρ on the lattice vectors of the photonic crystal. The effective wave equation for the envelope can thus be written as Eq. (8), which corresponds to the time-independent Schrödinger equation [14]

$$\left\{-\frac{\hbar^2\nabla^2}{2m^*} + V(\mathbf{x})\right\}\psi(\mathbf{x}) = E\,\psi(\mathbf{x}). \tag{8}$$

We will thus use the solution $\psi(\mathbf{x})$ as an approximation to $\Psi_n(\mathbf{x})$.

When the hole radius varies quadratically as a function of the distance from the center of the device, and the bottom ω_0 goes approximately linearly as a function of hole radius, the potential energy $V(\mathbf{x})$ becomes approximately harmonic. In this case, the solution of the Schrödinger equations are the well known harmonic oscillator states. In the following, we will compare the results of FDTD calculations with the results obtained in the local density approximation in one dimension. Subsequently, we will add disorder to the hole radius ρ_i. For this case, we will solve Eq. (8) for a distorted harmonic potential, and again compare the resulting $\psi(\mathbf{x})$ with FDTD calculations. We will conclude with the discussion of a two-dimensional example.

3. One-dimensional harmonic cavity

3.1. Effective mass and effective potential

In Fig. 1 the band structure of a one-dimensional photonic crystal is shown. This photonic crystal consists of dielectric slabs with a thickness $w = 0.45\,a$, where a denotes the lattice constant. The remaining 55 % of the unit cell consists of air. The band structure was obtained using the open-source MIT photonic band (MPB) package [18]. To a good approximation, the first band above the band gap in the dispersion relation around the edge of the first Brillouin zone can be taken to be parabolic. This means that we describe the energy of the electromagnetic modes with a dispersion that is similar to that of a massive particle

$$E(k) = E_0 + \frac{\hbar^2\,(k-k_0)^2}{2m^*}, \tag{9}$$

where E_0 denotes the energy of a photon at the minimum of the band, k_0 the wavenumber at the minimum of the band, and m^* the effective mass that arises from the local curvature of the band. Since we describe the local curvature in terms of an effective mass we include $\hbar$. This inclusion will make the relation to the Schrödinger equation more recognizable. Note however that despite the appearance of $\hbar$, our description is still completely classical.

Fitting a second order polynomial to the band in a small region around the minimum, and converting the scale invariant dimensionless units used by MPB to more conventional units, we

#228367 - $15.00 USD Received 11 Dec 2014; revised 27 Jan 2015; accepted 9 Feb 2015; published 13 Mar 2015

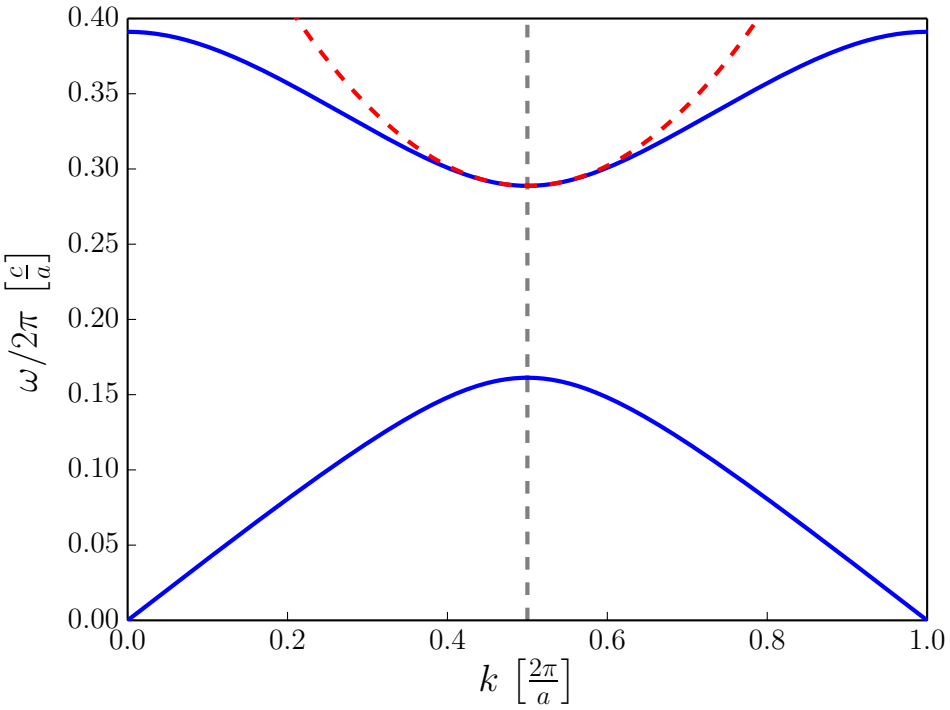

Fig. 1. Photonic band structure (blue) of a one-dimensional photonic crystal with a constant dielectric slab width of $w = 0.45\,a$. In red (dashed), a local parabolic approximation according to Eq. (9) is depicted. The vertical gray dashed line indicates the edge of the first Brillouin zone.

find $E_0 = 0.72\,\mathrm{eV}$ and $m^* = 1.82\,\mu m_\mathrm{e}$, where m_e denotes the electron mass. Here we have used a lattice constant $a = 500\,\mathrm{nm}$ and a dielectric constant $\varepsilon = 12$.

This calculation has been performed for a large range of widths w, resulting in Fig. 2. As shown in Fig. 2(a), the energy of a photon at the minimum of the band decreases for increasing slab width. Figure 2(b) shows the relation between the effective mass and the slab width. As can be seen from this figure, for small widths the effective mass increases for increasing slab width, passes through a maximum for $w \approx 0.38\,a$, and then decreases approximately linearly.

We now select a range of widths where m^* is approximately constant. The boundaries of the range are depicted by the vertical black dashed lines located at $w = 0.35\,a$ and $w = 0.45\,a$. For this range we find a clear linear dependence of E_0 on the width. Using this linear dependence, we construct our one-dimensional photonic crystal such that we slowly decrease the slab width away from its center ($w = 0.45$). This thus effectively results in a trapping potential for light in the crystal because the bands shift up when moving away from the center of the chirped photonic crystal.

By decreasing the slab size quadratically away from the center of the structure, the effective potential becomes harmonic since in our region of interest the dependence of E_0 on w is linear. Chirping the photonic crystal quadratically is achieved via

$$w(x) = w_0 - \left(\frac{x}{\eta}\right)^2, \tag{10}$$

#228367 - $15.00 USD Received 11 Dec 2014; revised 27 Jan 2015; accepted 9 Feb 2015; published 13 Mar 2015

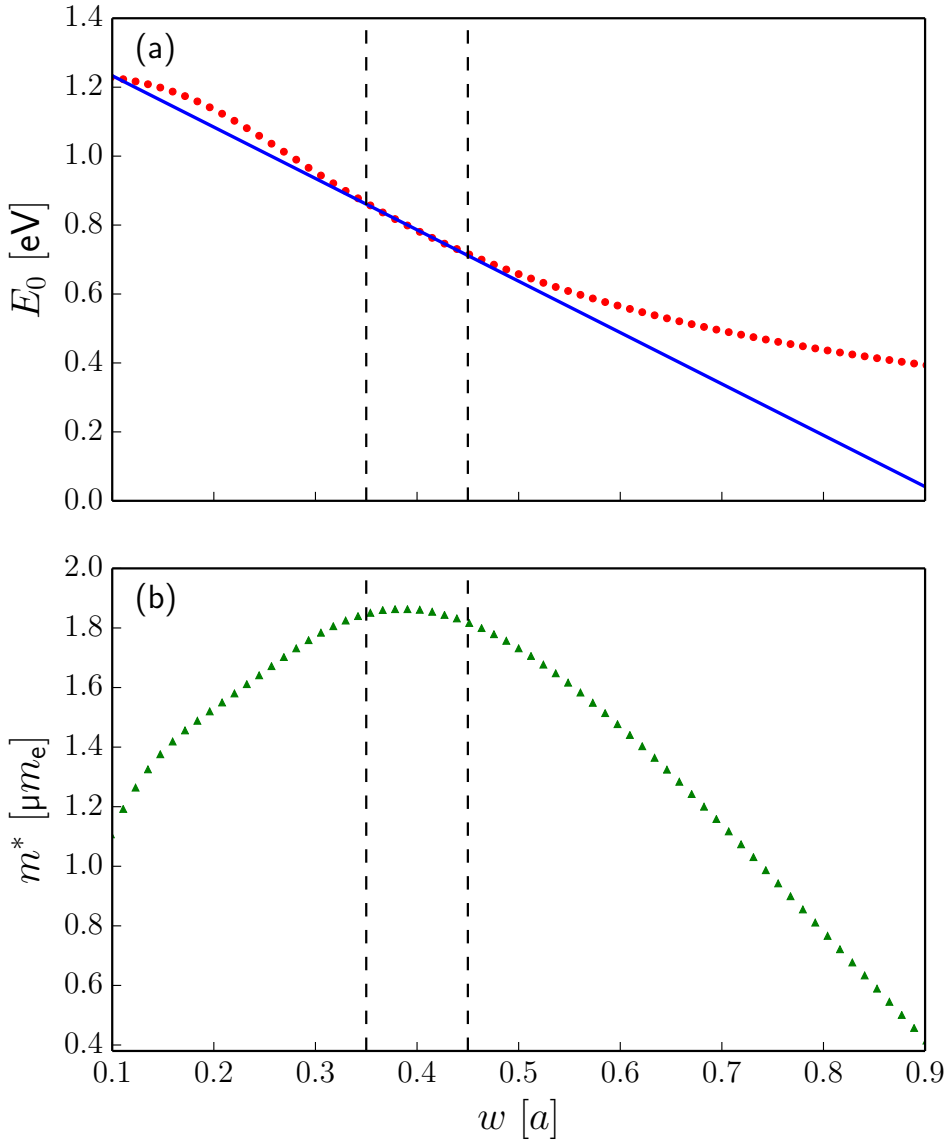

Fig. 2. MPB calculations for a range of slab widths w. In (a) the energy of the bottom of the band $E_0(w)$ (red circles) is depicted. A first order polynomial (blue) is fitted to the data points within the range depicted by the two vertical black dashed lines. In (b) the effective mass $m^*(w)$ is indicated by green triangles.

where $w(x)$ is treated as a continuous variable similar to Eq. (7), $w_0 = 0.45\,a$ denotes the slab width at the center of the structure, x the distance from the center, and η is a measure for the chirping of the photonic crystal. We use crystals described by Eq. (10) in FDTD simulations to investigate their electromagnetic mode profiles.

#228367 - $15.00 USD Received 11 Dec 2014; revised 27 Jan 2015; accepted 9 Feb 2015; published 13 Mar 2015

3.2. FDTD results

The simulation results discussed in this paper are obtained using the open source FDTD software package MEEP [19]. In an FDTD calculation, Maxwell's equations are evolved over time within a finite region. By analyzing the response of a system to a short pulse one can obtain frequencies, decay rates, and field patterns of the eigenmodes of a system.

For the simulations, the chirped photonic crystal is first initialized. In one dimension, this is achieved by setting a fraction of a unit cell to be dielectric material. For all photonic crystals discussed in this paper a dielectric constant $\varepsilon = 12$ is considered for the dielectric material. At the boundaries of the photonic crystal, a perfectly matched layer (PML) is added. The PML acts like an absorbing material that prevents reflections at the simulation boundaries. The photonic crystal including the PML is discretized in space and time by the resolution of the simulation. The resolution denotes the computational grid resolution, in pixels per unit distance.

Subsequently, we excite the eigenmodes of our photonic crystal using a short pulse with a center frequency f_{cen} and broad bandwidth f_Δ from a point current source (H_z), positioned inside the photonic crystal. This position will be referred to as the excitation point. During the evolution of the field inside the photonic crystal, the point current source is turned on. After the source is turned off, the field is evolved further and the resulting field at the location of the source is used to determine the frequencies $f_{\text{cen},n}$ of the eigenmodes using harmonic inversion [20]. In order to obtain the field patterns of an eigenmode, we run the simulation again using a pulse with a narrow-bandwidth f_δ around $f_{\text{cen},n}$. This way we excite only the mode in question.

Table 1. Simulation parameters for the one-dimensional chirped photonic crystal, where c denotes the speed of light. The value for the excitation point has been chosen such that it does not lie at the origin because this would result in the excitation of only the even ($n = 0, 2, 4, ...$) eigenmodes.

Parameter	Value
a	$500\,\text{nm}$
w_0	$0.45\,a$
η	$40\sqrt{a}$
resolution	$128\,\frac{\text{px}}{a}$
f_Δ	$0.2\,\frac{c}{a} = 120\,\text{THz}$
f_{cen}	$0.3\,\frac{c}{a} = 180\,\text{THz}$
f_δ	$0.001\,\frac{c}{a} = 600\,\text{GHz}$
excitation point	$-4.0\,a$

Using a single core of an Intel Core i3-2130 processor, calculating the field pattern of a single mode in one dimension takes $\approx 8.4\,\text{min}$ for the values listed in Table 1. In Fig. 3, the resulting field patterns of the first four eigenmodes of the photonic crystal are shown in blue. In this figure the dielectric function of the photonic crystal is depicted in gray. From this figure we see that the magnetic field component (H_z) is confined to the dielectric slabs. Also, for each successive eigenmode we observe additional nodes in the apparent envelope of the field pattern. These apparent envelopes strongly resemble the quantum harmonic oscillator modes [21]. We quantify this resemblance in the next sections.

#228367 - $15.00 USD Received 11 Dec 2014; revised 27 Jan 2015; accepted 9 Feb 2015; published 13 Mar 2015

3.3. Local density results

As mentioned in Sec. 3.1, the potential can be approximated to be harmonic when the photonic crystal is chirped quadratically. In the one-dimensional case, Eq. (8) can thus be written as

$$-\frac{\hbar^2}{2m^*}\frac{d^2\psi(x)}{dx^2}+\frac{1}{2}m^*\Omega^2x^2\psi(x)=(E-V(0))\,\psi(x), \tag{11}$$

where Ω denotes the harmonic oscillator frequency, and $V(0)$ the potential energy at $x=0$.

The eigenvalues and eigenfunctions of this equation are well known and are given by [21]

$$E_{n'}=V(0)+\hbar\Omega\left(n'+\frac{1}{2}\right), \tag{12}$$

and

$$\psi_{n'}(x)=\left(\frac{m^*\Omega}{\pi\hbar}\right)^{1/4}\frac{1}{\sqrt{2^{n'}n'!}}H_{n'}(\xi)\mathrm{e}^{-\xi^2/2}, \tag{13}$$

where $H_{n'}(\xi)$ denotes the n'-th Hermite polynomial, and $\xi=x/l_{\mathrm{HO}}$ a dimensionless variable with $l_{\mathrm{HO}}=\sqrt{\hbar/m^*\Omega}$ the harmonic oscillator length. Using the values for a and η from Table 1, we find $\Omega=2\pi\cdot 4.23\,\mathrm{THz}$ and $l_{\mathrm{HO}}=1.53\,\mu\mathrm{m}$.

In Fig. 3 the squared absolute value of the wavefunctions (red-dashed) of Eq. (13) are plotted using these values. The wavefunctions show an excellent correspondence with the apparent envelope of the field patterns obtained by the FDTD simulation. As explained in Section 3.1, the key to the local density approach is the fact that the effective mass m^* can be considered constant for a large enough range of widths w. To map the envelope function we furthermore require a linear relation between the energy of the bottom of the band E_0 and w. Since the higher order modes extend further towards the outside of the structure, they are more sensitive to deviations from these ideal conditions. For higher order modes we therefore observe a mismatch between the envelopes obtained in the local density approach and the exact envelope obtained from FDTD.

To quantify the agreement between the FDTD simulation and the quantum harmonic oscillator modes, we first compare the mode frequency spacings. From the FDTD simulation we obtain a mode frequency spacing of $2\pi\cdot 3.82\,\mathrm{THz}$ between $f_{\mathrm{cen},0}$ and $f_{\mathrm{cen},1}$. As mentioned above, the local density approximation yields $\Omega=2\pi\cdot 4.23\,\mathrm{THz}$. This amounts to a difference of 10 % which already shows a good agreement.

3.4. Detailed analysis of the local density results

In the previous section we have seen promising results from our local density approach. However, what we are interested in are the mode profiles of photonic crystals while avoiding time consuming FDTD calculations. In this section we therefore determine the agreement between the envelope $\Psi_n(x)$ of the eigenmodes obtained from FDTD simulations and the quantum harmonic oscillator modes $\psi_{n'}(x)$. We do this by computing the inner product

$$c_{n,n'}=\langle\Psi_n(x)|\psi_{n'}(x)\rangle\,, \tag{14}$$

where $c_{n,n'}$ thus denotes the contribution of $\psi_{n'}(x)$ to $\Psi_n(x)$.

To determine $c_{n,n'}$ we must first obtain the envelope function $\Psi_n(x)$ from the FDTD simulations. We do this by spatially Fourier transforming the field pattern, retrieving the components of the field in reciprocal space, *i.e.* the Fourier transform of Eq. (6). In the case of a one-dimensional photonic crystal, $\{\mathbf{k}_{\mathrm{min}}\}$ corresponds to the edges of the first Brillouin zone. In Fig. 4(b), the spatial Fourier transform is shown (blue solid line) of the fundamental mode of the field pattern in Fig. 4(a).

#228367 - $15.00 USD Received 11 Dec 2014; revised 27 Jan 2015; accepted 9 Feb 2015; published 13 Mar 2015

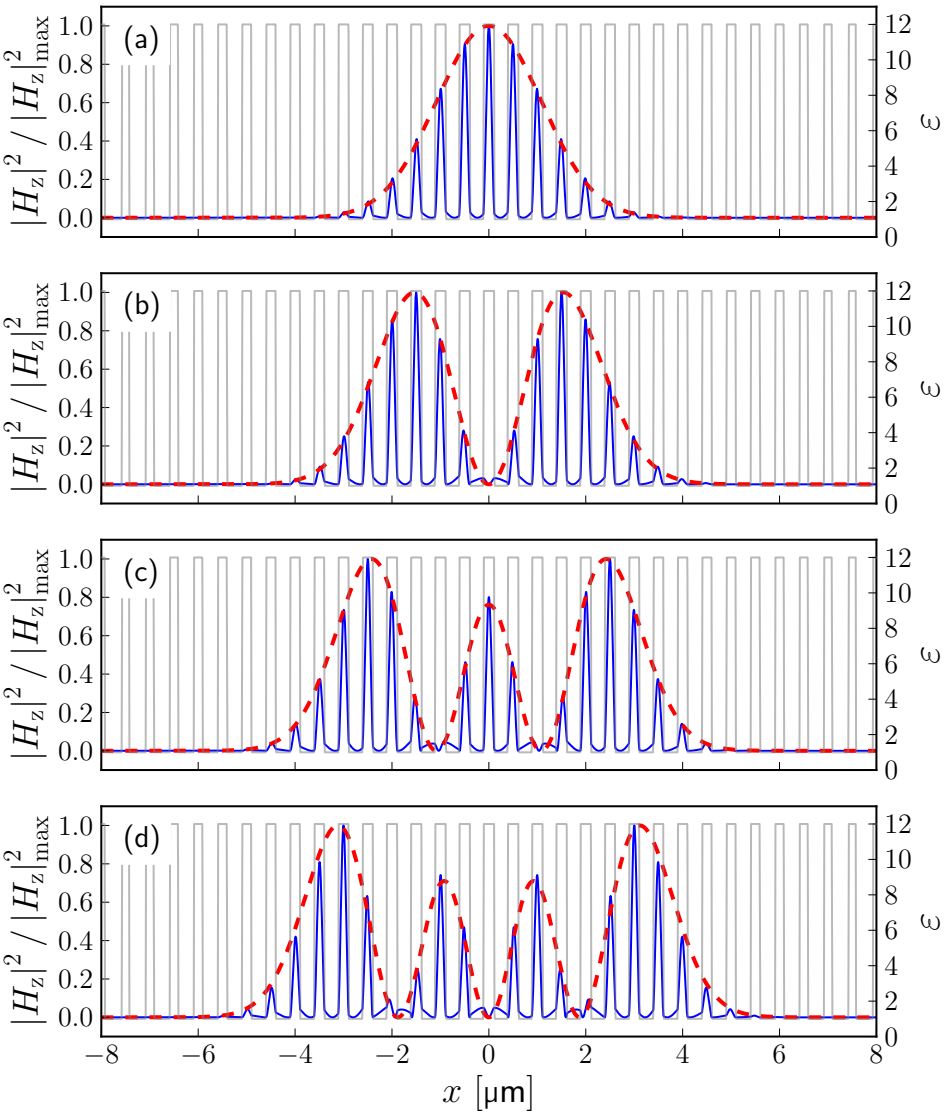

Fig. 3. FDTD results of the field patterns in one dimension for (a) the first, (b) the second, (c) the third, and (d) the fourth eigenmode. The intensity of the field patterns (blue) are plotted as a function of position x. The absolute squared eigenmodes of the quantum harmonic oscillator (red dashed) are plotted. In the background the dielectric function $\varepsilon(x)$ (gray) of the photonic crystal is plotted, its value indicated on the right axis.

The spatial Fourier transformation of Eq. (6) can be written as

$$\tilde{\mathbf{H}}_{m_c}(\mathbf{k}) = \tilde{\Psi}_n(\mathbf{k}) \otimes \tilde{\mathscr{H}}_{m_c,\mathbf{k}_{\min}}(\mathbf{k}), \tag{15}$$

where $\otimes$ denotes a convolution and

$$\tilde{\mathscr{H}}_{m_c,\mathbf{k}_{\min}}(\mathbf{k}) = \sum_{\mathbf{k}_{\min},\kappa} \tilde{\mathscr{H}}_{\mathbf{k}_{\min},\kappa} \delta\left(\mathbf{k} - (\mathbf{k}_{\min} + \kappa)\right), \tag{16}$$

#228367 - $15.00 USD Received 11 Dec 2014; revised 27 Jan 2015; accepted 9 Feb 2015; published 13 Mar 2015

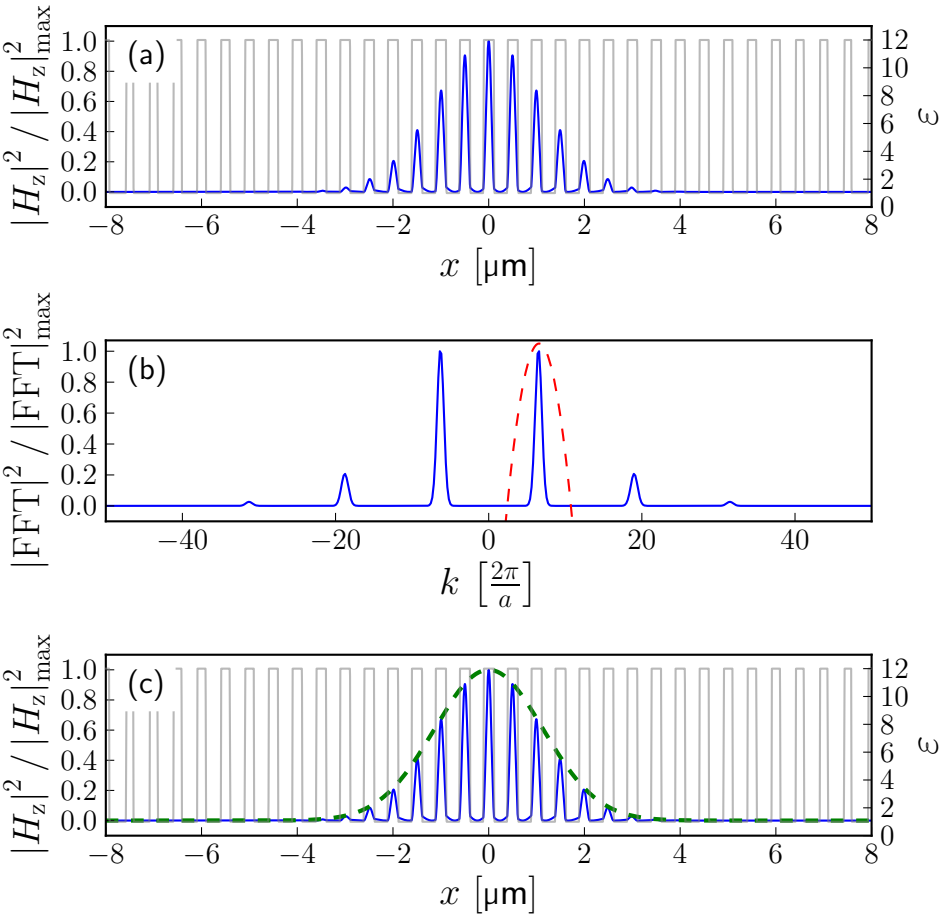

Fig. 4. Obtaining the envelope of an eigenmode of the chirped photonic crystal. In (a) the complex field pattern (blue) of Fig. 3(a) is depicted. In (b) the spatial Fourier transform (blue) of (a) is shown. A mask (red dashed) is centered at the edge of the first Brillouin zone. Multiplying (b) with the complex conjugate of the corresponding plane wave, and taking the inverse Fourier transform results in (c). Here, the resulting envelope Ψ_0 is indicated by the green dashed line.

where $\kappa = i\mathbf{a}^* + j\mathbf{b}^*$ with $\mathbf{a}^*$ and $\mathbf{b}^*$ the reciprocal lattice vectors, and i, $j \in \mathbb{Z}$.

Placing a mask as indicated by the red dashed curve in Fig. 4(b) over the positive valued $\mathbf{k}_{\min}$ of the first Brillouin zone, Eq. (15) is reduced to

$$\tilde{\mathbf{H}}_{\mathrm{mask},m_c}(\mathbf{k}) = \tilde{\Psi}_n(\mathbf{k}) \otimes \tilde{\mathscr{H}}_{m_c,\mathbf{k}_{\min}} \delta\left(\mathbf{k} - \mathbf{k}_{\min}\right), \tag{17}$$

where $\tilde{\mathbf{H}}_{\mathrm{mask},m_c}(\mathbf{k})$ denotes the masked Fourier transform of the magnetic field.

Taking the inverse Fourier transform of Eq. (17), and multiplying the result with the complex conjugate of a plane wave with wavevector $\mathbf{k}_{\min}$, in order to eliminate the exponential term, yields the envelope $\Psi_n(x)$ as indicated by the green dashed line in Fig. 4(c).

Now, the contributions of $\psi_{n'}(x)$ to $\Psi_n(x)$ can be determined. As an example, the contributions of $\psi_{n'}(x)$ to the third eigenmode of the FDTD simulation ($n = 2$) are shown in Fig. 5.

From Fig. 5 we observe a very good agreement between the envelope (a) and corresponding

#228367 - $15.00 USD Received 11 Dec 2014; revised 27 Jan 2015; accepted 9 Feb 2015; published 13 Mar 2015

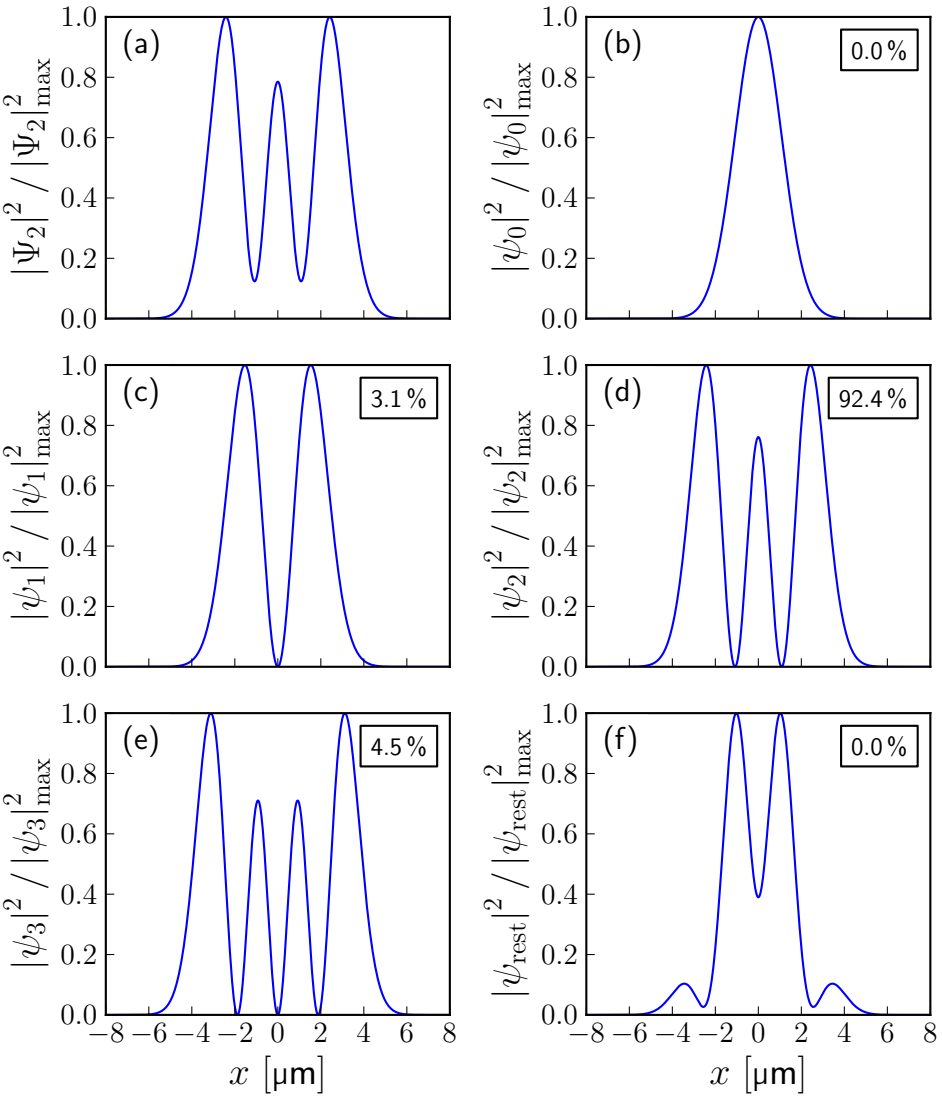

Fig. 5. Envelope of a single mode Ψ_n compared to all theoretical harmonic modes $\psi_{n'}$. In (a) the envelope of the third eigenmode Ψ_2, (b) the first harmonic ψ_0, (c) the second harmonic ψ_1, (d) the third harmonic ψ_2, (e) the fourth harmonic ψ_3, (f) all other harmonic modes ψ_{rest}. In the upper right corner of subplots (b) - (f) the contribution $|c_{2,n'}|^2$ of $\psi_{n'}$ to Ψ_2 is depicted.

eigenmode of the quantum harmonic oscillator (d): $|c_{2,2}|^2 = 92.4\,\%$. We also observe that the neighboring eigenmodes of the quantum harmonic oscillator $\psi_1(x)$ and $\psi_3(x)$ show a contribution of a few percent. This is likely because the zero crossings of the $n = 2$ harmonic oscillator wavefunctions are close to the maxima of the Bloch function of the magnetic field which leads to a local violation of the local density approximation. Quantitative analysis of the electric field, of which the Bloch function already has a minimum at those zero crossings, supports this statement, as for the electric field the envelope much more closely approaches the quantum

#228367 - $15.00 USD Received 11 Dec 2014; revised 27 Jan 2015; accepted 9 Feb 2015; published 13 Mar 2015

harmonic oscillator.

For the one-dimensional case, the modes found from the FDTD simulations are thus in excellent ($> 90\,\%$) quantitative agreement with the eigenmodes of the quantum harmonic oscillator.

3.5. One-dimensional harmonic cavity with disorder

We have just seen that the FDTD simulations for a chirped photonic crystal show an excellent agreement with the corresponding solutions of the one-dimensional time-independent Schrödinger equation. However, fabricated photonic crystals will not be perfect in the sense that the diameter and position of the air holes can deviate from their intended value. These fabrication imperfections result in a distorted harmonic potential.

For a fabrication error on the position Δx of the air holes, the local effective refractive index of the photonic crystal is comparable to that of the perfect quadratically chirped photonic crystal. In the band structure of Fig. 1 this means that there is a small displacement in the $\pm k$-direction at the bottom of the band. Since this is a local minimum, E_0 is unaltered up to first order in k. However, in the same figure a fabrication error on the diameter $\Delta w(x_i)$ of the air holes results in a vertical shift *i.e.* a change of E_0. Hence, this vertical shift has a much stronger effect on the distortion of the harmonic potential than that of the horizontal shift at the bottom of the band. For the distorted harmonic potential we therefore only consider fabrication imperfections on the diameter of the air holes.

Including fabrication imperfections, the photonic crystal is described by

$$w(x_i) = w_0 - \left(\frac{x_i}{\eta}\right)^2 + \Delta w(x_i), \tag{18}$$

where we now cannot treat w as a continuous variable as the hole size deviation only has a single value per unit cell.

In Fig. 6, the first four eigenmodes are plotted (blue) for a photonic crystal created using Eq. (18). Here $\Delta w(x_i)$ is generated using a random number generator that is normally distributed with a standard deviation of $\sigma_w = 10\,\text{nm}$. Again, the magnetic field component (H_z) is confined to the dielectric slabs, but as can be seen from the figure, the field patterns deviate considerably from those of the ideal system shown in Fig. 3. From the apparent envelopes of the field patterns in Fig. 6 a monotonic increase of the number of nodes with the mode number is still visible. However, there is no longer a symmetry plane through the origin.

In our model this is because the potential is no longer harmonic. Taking into account the fabrication imperfections the potential can be expressed as

$$V(x_i) = \frac{1}{2} m^* \Omega^2 x_i^2 + \Delta V(\Delta w(x_i)), \tag{19}$$

where $\Delta V(\Delta w(x_i))$ denotes the distortion of the harmonic potential due to $\Delta w(x_i)$.

Solving Schrödinger's equation with the potential as given by Eq. (19) can be achieved using normalized Numerov integration [22]. Numerov integration is a numerical method for solving second order differential equations without a first order term. As we only know V on one point per unit cell, we perform the Numerov integration using a single grid point per unit cell. For comparison with time-consuming FDTD simulations, finding four modes using Numerov integration takes a few seconds.

The results of the Numerov integration are indicated by the green dashed line in Fig. 6. The green dots depict the grid points used for the integration. As can be seen from this figure there is an excellent agreement between the solutions of the normalized Numerov integration method and the envelopes of the eigenmodes for a distorted chirped photonic crystal.

#228367 - $15.00 USD Received 11 Dec 2014; revised 27 Jan 2015; accepted 9 Feb 2015; published 13 Mar 2015

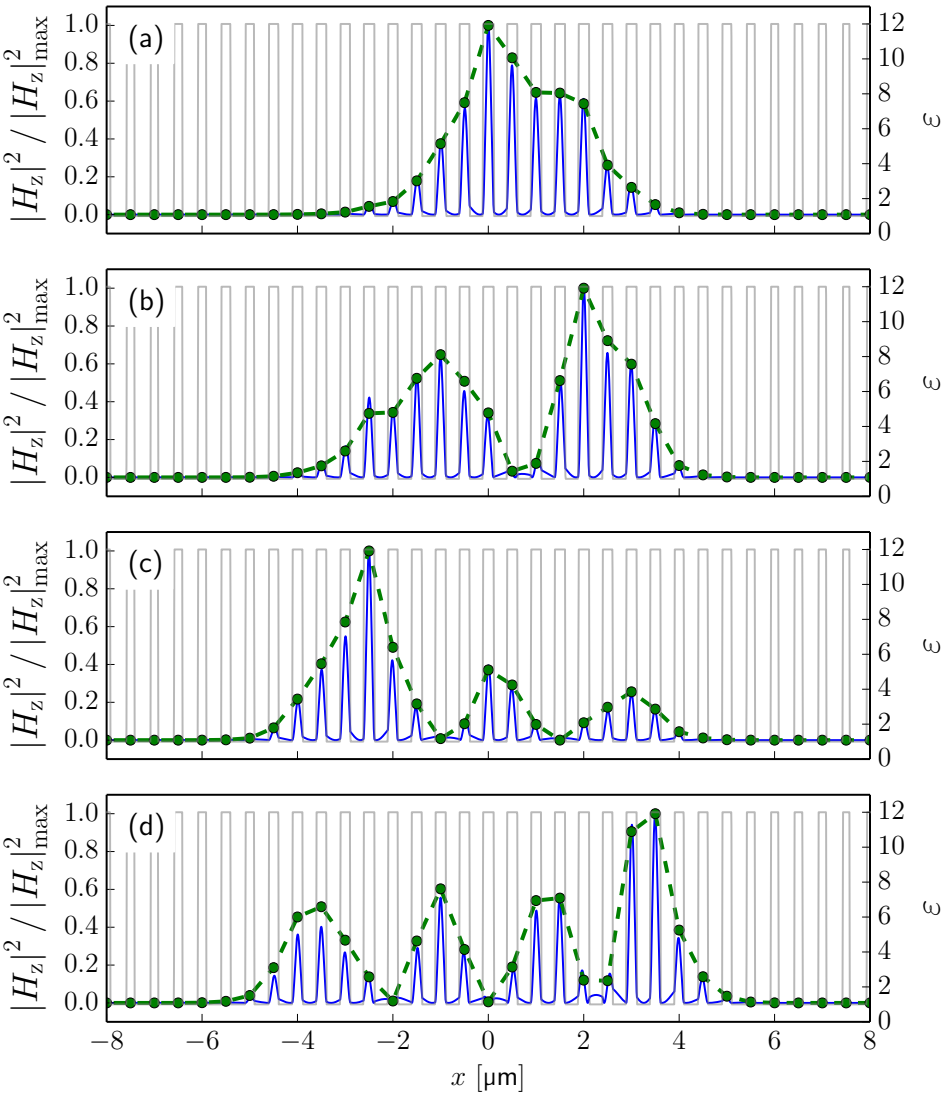

Fig. 6. FDTD results of the field patterns in one dimension with a distorted harmonic potential. The intensity of the field patterns (blue) are plotted as a function of position x for (a) the first, (b) second, (c) third, and (d) fourth eigenmode. In each subfigure, the normalized Numerov integration (green dashed) is included. The green dots depict the grid points used for this integration. In the background the dielectric function $\varepsilon(x)$ (gray) of the photonic crystal is plotted, its value indicated on the right axis.

In one dimension we have shown that the eigenmodes of a perfect quadratically chirped photonic crystal can be mapped to the eigenmodes of the quantum harmonic oscillator with a typical agreement of $> 90\,\%$. When adding disorder to the photonic crystal, its eigenmodes can still be approximated by the solutions of the Schrödinger equation which are obtained using the normalized Numerov integration scheme.

#228367 - $15.00 USD Received 11 Dec 2014; revised 27 Jan 2015; accepted 9 Feb 2015; published 13 Mar 2015

4. Two-dimensional harmonic cavity

4.1. Effective mass and effective potential

We now extend our approach to two dimensions. Analogous to the one-dimensional case, the photonic crystal needs to be designed such that a complete photonic band gap arises, the effective mass can be considered constant, and gives rise to an effective harmonic potential.

Two-dimensional photonic crystals are periodic in a certain plane while they are uniform in the direction perpendicular to that plane. We define this plane to be the xy-plane. Due to mirror symmetry of the crystal in this plane the modes can be classified into two distinct polarization classes. When the electric field is confined to the xy-plane the modes are referred to as being transverse electric (TE). Its polarization is given by (E_x, E_y, H_z). When the magnetic field is confined to the xy-plane the modes are assigned transverse magnetic (TM). The corresponding polarization is given by (H_x, H_y, E_z).

We compute the band structure for a two-dimensional photonic crystal consisting of a triangular lattice of air holes. In Fig. 7 we show the band structure for a photonic crystal with an air hole radius of $\rho = 0.42a$.

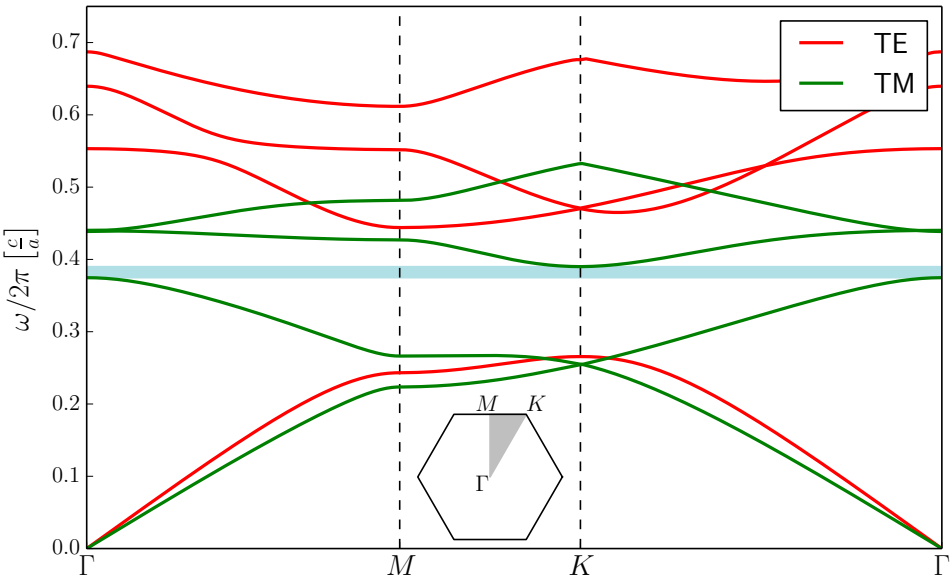

Fig. 7. Photonic band structure with the TE (red) and TM (green) bands of a two-dimensional photonic crystal consisting of a triangular lattice of air holes. The radius of the air holes equals $\rho = 0.42a$. The blue horizontal region depicts the complete photonic band gap.

With $\rho = 0.42a$ a complete photonic band gap is obtained such that no light in a certain frequency range can propagate through the crystal. This band gap is indicated by the blue horizontal region in Fig. 7. Increasing ρ will increase the size of the band gap. The first minimum of the band above the band gap is located in the third TM band. Hence, an E_z source can be used to excite the mode within this band.

Also indicated in Fig. 7 is the hexagonally shaped Brillouin zone. The irreducible part of the Brillouin zone is indicated by the gray shaded area. Within the Brillouin zone there are three high symmetry points: Γ, M, and K. As can be observed from the band structure the minimum of the third TM band is located at a K-point.

#228367 - $15.00 USD Received 11 Dec 2014; revised 27 Jan 2015; accepted 9 Feb 2015; published 13 Mar 2015

From the curvature of the band around the minimum, we can again determine the effective mass. However, assigning a single effective mass is problematic in two- and three-dimensional crystals as the effective mass generally depends on the direction. In this specific case, the dispersion is almost isotropic around the K-point; the effective mass varies only a few percent as a function of direction. For this reason, we use in the following the angle averaged effective mass.

In one dimension we have seen that by chirping the photonic crystal in a quadratic manner, an effective harmonic potential is obtained. Quadratically chirping a two dimensional crystal can be achieved by replacing Eq. (10) with

$$\rho(x,y) = \rho_0 + \frac{1}{2}\left(\frac{x^2+y^2}{\eta^2}\right), \tag{20}$$

where $\rho(x,y)$ is again treated as a continuous variable similar to Eq. (7), and ρ_0 denotes the radius of the center air hole. Note that the crystal is now described in terms of the air hole radius rather than the dielectric slab width as in Eq. (10).

Chirping the photonic crystal according to Eq. (20), the resulting two-dimensional harmonic potential is given by

$$V(x,y) = \frac{1}{2}m^*\Omega^2(x^2+y^2). \tag{21}$$

With this harmonic potential the solutions of the two-dimensional time-independent Schrödinger equation are obtained. These solutions are used to investigate our model in two dimensions, *i.e.* to determine their overlap with the envelopes of the corresponding eigenmodes of the photonic crystal found by performing FDTD simulations.

4.2. Results

In order to excite the mode within the third TM band we use an E_z source as mentioned in Sec. 4.1. For a simple comparison of the computational effort, we ran the simulation on a single core of an Intel Core i3-2130 processor using the parameters listed in Table 2. Per eigenmode of the photonic crystal, this results in a computation time of $\approx 6.5\,\mathrm{h}$.

Table 2. Simulation parameters for the two-dimensional chirped photonic crystal. The excitation point is given as (x, y). The value for the excitation point has been chosen such that it does not lie on a symmetry axis of the photonic crystal because this would result in the excitation of only the even ($n = 0,2,4,\ldots$) eigenmodes.

Parameter	Value
a	$500\,\mathrm{nm}$
ρ_0	$0.405\,a$
η	$40\sqrt{a}$
resolution	$32\,\frac{\mathrm{px}}{a}$
f_Δ	$0.03\,\frac{c}{a} = 18\,\mathrm{THz}$
f_{cen}	$0.38\,\frac{c}{a} = 228\,\mathrm{THz}$
f_δ	$0.001\,\frac{c}{a} = 600\,\mathrm{GHz}$
excitation point	$(-1.775\,a, -1.044\,a)$

In two dimensions, the time-independent Schrödinger equation in polar coordinates is given by

$$\left\{-\frac{\hbar^2}{2m^*}\left[\frac{\partial^2}{\partial r^2} + \frac{1}{r}\frac{\partial}{\partial r} + \frac{1}{r^2}\frac{\partial^2}{\partial \phi^2}\right] + V(r)\right\}\psi_{n',l} = E\,\psi_{n',l}, \tag{22}$$

#228367 - $15.00 USD Received 11 Dec 2014; revised 27 Jan 2015; accepted 9 Feb 2015; published 13 Mar 2015

where $V(r) = \frac{1}{2}m^*\Omega^2 r^2$ denotes the harmonic potential, and Ω the harmonic oscillator frequency. The subscripts n' and l denote the principle quantum number and the quantum number related to the z-component of the angular momentum, respectively.

The solutions of Eq. (22) are given by [23]

$$\psi_{n',l}(r,\phi) = C_{n',l}e^{-\zeta^2/2}(\zeta)^{|l|}L_p^{|l|}(\zeta^2)e^{il\phi}, \tag{23}$$

where $L_p^{|l|}(\zeta^2)$ denotes the generalized Laguerre polynomials, $p = \frac{n'-|l|}{2}$ the radial quantum number, $\zeta \equiv \sqrt{\frac{m^*\Omega}{\hbar}}r$ a dimensionless variable, and $C_{p,l} = \sqrt{\frac{2m^*\Omega p!}{\hbar(p+|l|)!}}$ a normalization constant.

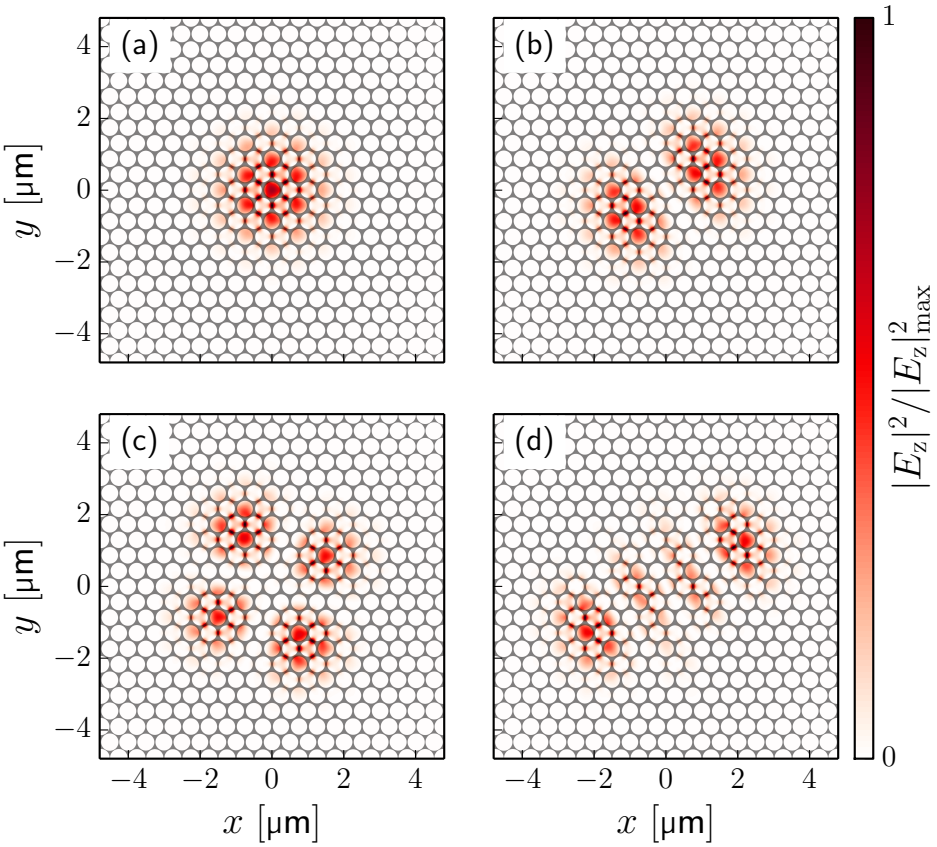

Fig. 8. FDTD results of the field patterns in two dimensions. From white to dark red, the intensity of the field patterns are plotted for (a) the first, (b) the second, (c) the third, and (d) the fourth eigenmode. On top of the field patterns the chirped photonic crystal is plotted, where the dielectric material is depicted in black and the air holes in white.

The solutions $\psi_{n',l}(r,\phi)$ are complex valued functions, whereas MEEP by default returns real valued fields. Complex field patterns can be obtained using MEEP. In this case both the simulation time per mode and the memory usage are increased by a factor 2. A more elegant way to obtain the complex valued fields is to use a Fourier transformation from the time domain to the frequency domain of the FDTD field patterns. In the frequency domain we discard the negative frequency components as they are not a solution to Schrödinger's equation. By taking

#228367 - $15.00 USD Received 11 Dec 2014; revised 27 Jan 2015; accepted 9 Feb 2015; published 13 Mar 2015

the inverse Fourier transform to return to the time domain, we recover the complex valued field patterns.

In Fig. 8 the intensity of the first four eigenmodes is depicted, ranging from white to dark red. The modes have been normalized to unity as indicated by the colorbar. On top of each eigenmode the photonic crystal structure is drawn.

To determine the envelopes of the eigenmodes in Fig. 8, we again take the spatial Fourier transform of the complex valued field pattern. The result of this Fourier transform is given in Fig. 9(a), where the maximum intensities are distributed in a hexagonal manner due to a six-fold rotational symmetry of the crystal. We select one of the intensity maxima using a mask (blue dashed circle). Taking the inverse Fourier transform, and multiplying the result with the complex conjugate of a plane wave with wavevector $\mathbf{k}_{\text{min}}$ yields the envelope $\Psi_n(r,\phi)$, as indicated in Fig. 9(b).

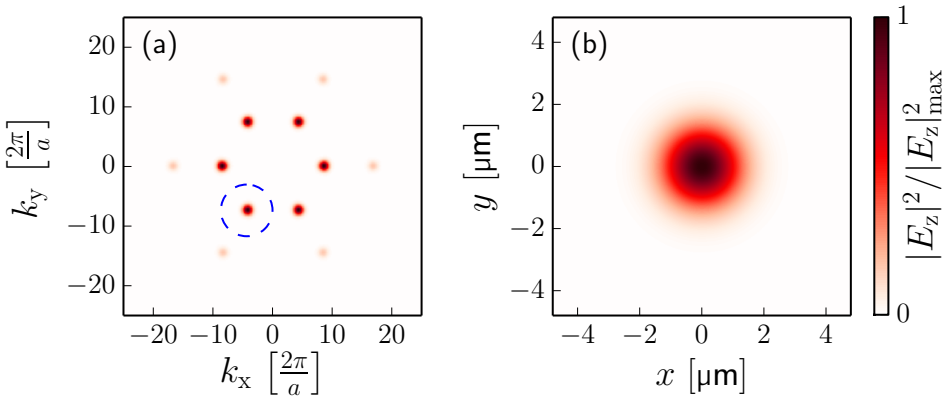

Fig. 9. Obtaining the envelope of an eigenmode of the chirped photonic crystal cavity. In (a) the spatial Fourier transform of the field pattern of Fig. 8(a) is shown. A mask (blue dashed) is placed around an intensity maxima. Taking the inverse Fourier transform, and multiplying the result with the complex conjugate of the corresponding plane wave results in the envelope $\Psi_n(r,\phi)$ in (b).

However, before we determine the overlap between the FDTD envelopes and the eigenmodes of the quantum harmonic oscillator we first note that for each principal quantum number $n' = 2p + |l|$ the eigenmodes of the quantum harmonic oscillator have a $(n'+1)$-fold degeneracy. Due to this degeneracy, we expect the mode envelopes to be described by a superposition of degenerate quantum harmonic oscillator modes, *i.e.*

$$\psi_{n'}(r,\phi) = \sum_l c_{n,\{n',l\}}\,\psi_{n',l}(r,\phi), \tag{24}$$

where $c_{n,\{n',l\}}$ denotes the contribution of each degenerate state $\psi_{n',l}(r,\phi)$ to $\Psi_n(r,\phi)$. This contribution is determined via

$$c_{n,\{n',l\}} = \left\langle \Psi_n(r,\phi) | \psi_{n',l}(r,\phi) \right\rangle. \tag{25}$$

The total contribution of the eigenmodes of the quantum harmonic oscillator to the mode envelopes of the FDTD simulations is expressed by

$$\left|c_{n,n'}\right|^2 = \sum_l \left|c_{n,\{n',l\}}\right|^2. \tag{26}$$

#228367 - $15.00 USD Received 11 Dec 2014; revised 27 Jan 2015; accepted 9 Feb 2015; published 13 Mar 2015

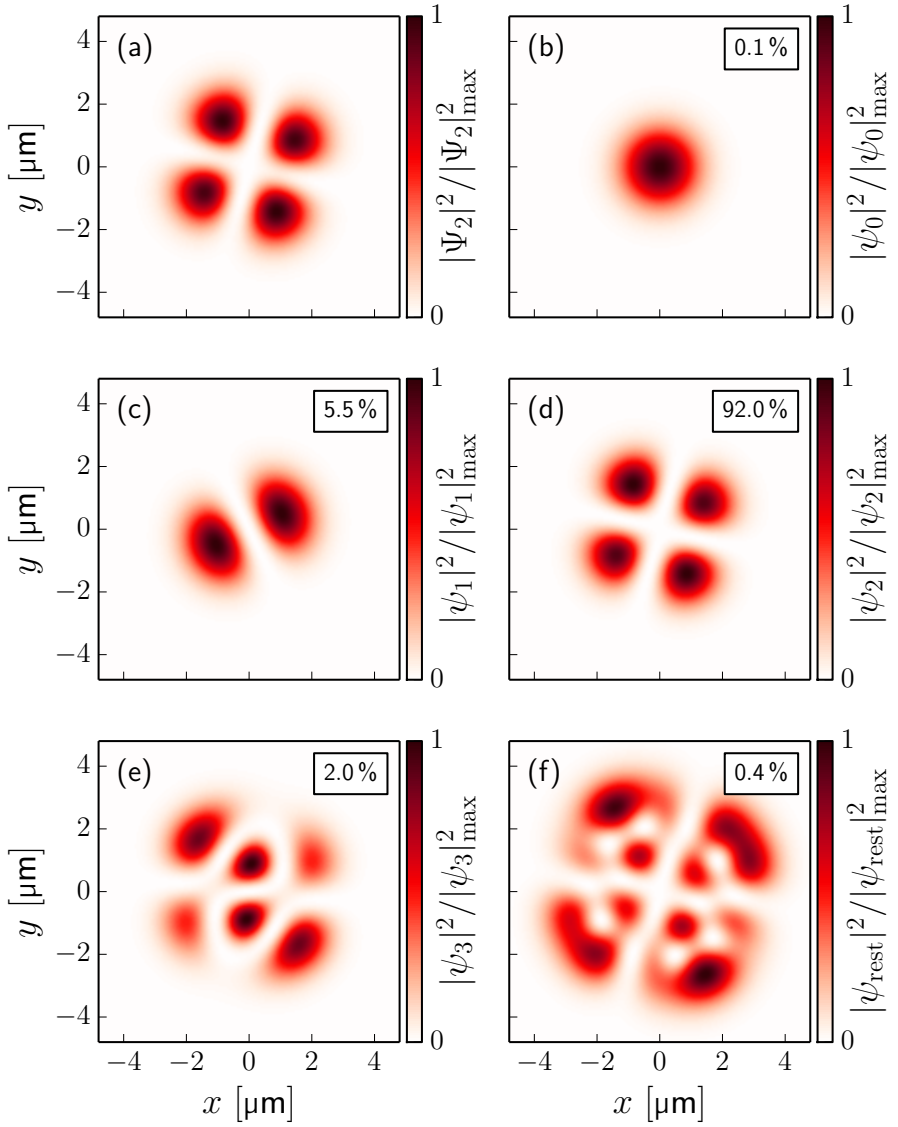

Fig. 10. Envelope of a single mode Ψ_n compared to all theoretical harmonic modes $\psi_{n'}$. In (a) the envelope of the third eigenmode Ψ_2, (b) the first harmonic ψ_0, (c) the second harmonic ψ_1, (d) the third harmonic ψ_2, (e) the fourth harmonic ψ_3, (f) all other harmonic modes ψ_{rest}. In the upper right corner of subplots (b) - (f) the contribution $|c_{2,n'}|^2$ of $\psi_{n'}$ to Ψ_2 is depicted.

In Fig. 10 the contributions of the eigenmodes $\psi_{n'}(r,\phi)$ of the quantum harmonic oscillator to $\Psi_2(r,\phi)$ are shown. In the upper right corner of (b)-(f), $\left|c_{2,n'}\right|^2$ is indicated for each mode. Similar to one dimension, there is an excellent agreement ($|c_{2,2}|^2 = 92.0\,\%$) between the envelope of the third eigenmode of the FDTD simulation and the third eigenmode of the quantum harmonic oscillator. The neighboring modes again have contributions of only a few percent. For

#228367 - $15.00 USD Received 11 Dec 2014; revised 27 Jan 2015; accepted 9 Feb 2015; published 13 Mar 2015

the two-dimensional photonic crystal, the eigenmodes obtained from the FDTD simulations can thus be described in excellent ($> 90\,\%$) agreement by the eigenmodes of the two-dimensional quantum harmonic oscillator.

5. Conclusions

We demonstrated a novel and intuitive approach to calculate the electromagnetic field modes of photonic crystals by translating this task to solving a simple time-independent Schrödinger equation, thereby avoiding large computational FDTD simulations.

For this approach the local potential energy within a chirped photonic crystal was derived from the energy of the bottom of a photonic band for a periodic photonic crystal. The effective mass was obtained from the curvature of this band. We have shown that for a certain range of air hole radii, the energy at the bottom of the band decreases linearly with the air hole radius, whereas the effective mass can be considered constant to a good approximation. Increasing the air hole radius quadratically as a function of distance to the center of the crystal results in an effective harmonic potential.

With this harmonic potential, we obtained the solutions of the time-independent Schrödinger equation. Comparing these solutions in both one and two dimensions to the envelopes of the eigenmodes within the photonic crystals, yields a typical overlap well above $90\,\%$. The analytical solutions of the time-independent Schrödinger equation can thus be used to model the eigenmodes of one- and two-dimensional photonic crystals to a very good approximation. This approach reduces computational effort by many orders of magnitude.

We have also shown that adding disorder to the photonic crystal in the form of a deviation on the air hole radius results in a distorted potential. Using normalized Numerov integration we solved the time-independent Schrödinger equation with this potential using only a single grid point per unit cell. The solutions follow the envelopes of the corresponding field patterns of the FDTD simulations. Our approach thus even works in the presence of disorder.

Our technique could be extended to increase the accuracy for higher order modes. As explained a mismatch occurs because the linear relation for $E_0(w)$ breaks down and the effective mass m^* can no longer be considered constant. In this case numerical integration can be performed to account for the non-linearity of $E_0(w)$. Also, a position dependent mass could be included in this integration to obtain a more accurate calculation of the envelope. This is however beyond the scope of this work.

Due to the intuitive nature and low computational costs of the model it can be of great interest when designing large photonic crystal structures, for instance in the field of photovoltaics, optoelectronics, and solid-state lighting.

Acknowledgment

This work is part of the research program of the Foundation for Fundamental Research on Matter (FOM), which is part of the Netherlands Organization for Scientific Research (NWO).

#228367 - $15.00 USD Received 11 Dec 2014; revised 27 Jan 2015; accepted 9 Feb 2015; published 13 Mar 2015